
Proceedings Paper:
Smith, M.J., Gladwin, D.T. and Stone, D.A. (2017) Experimental Analysis of the Influence of High-Frequency Ripple Currents on Dynamic Charge Acceptance in Lead-Acid Batteries. In: IECON 2017 - 43rd Annual Conference of the IEEE Industrial Electronics Society. 43rd Annual Conference of the IEEE Industrial Electronics Society, 29 Oct - 01 Nov 2017, Beijing, China. IEEE, pp. 7140-7145. ISSN: 1553-572X.

https://doi.org/10.1109/IECON.2017.8217249

Experimental Analysis of the Influence of High-Frequency Ripple Currents on Dynamic Charge Acceptance in Lead-Acid Batteries

M. J. Smith, D. T. Gladwin and D. A. Stone
Electrical Machines and Drives Research Group,
Department of Electronic and Electrical Engineering,
University of Sheffield, Sheffield, UK
Email: matt.j.smith@sheffield.ac.uk

***Abstract*—This paper presents the results of a series of tests to determine the influence of high-frequency injected ripple currents on the Dynamic Charge Acceptance (DCA) performance of lead-acid batteries. A wide-bandwidth battery model is described, this being a hybrid of the standard Randles model and a high-frequency model previously described in literature. A bespoke test procedure is described, based on the existing DCA Short Test profile. The results demonstrate that the injection of ripple currents can significantly improve charge acceptance.**

I. Introduction

There has been a major shift over recent years in the use of batteries in automotive applications. Traditionally the battery has been used exclusively as an auxiliary energy store, nowadays the use of the battery purely for starting, lighting and ignition (SLI) is becoming increasingly rare. Environmental and economic concerns mean the internal combustion engine is run less, utilising either start-stop or hybrid electric vehicle (HEV) technology; or eliminated altogether in the case of fully electric vehicles (EV). Concurrently, vehicles are becoming more power-hungry, with increasingly complex on-board driver aids, entertainment and HVAC systems. These changes make the performance of the battery fundamental to the overall performance of the vehicle.

A key area of interest stemming from this change has been the study of Dynamic Charge Acceptance (DCA) in batteries. This is important because the nature of the operating environment for EV and HEV batteries means they are often subjected to very high rates of charge, up to 30 times the 1-hour rate (C_1), during regenerative braking [1]. Overall battery effectiveness under these conditions is determined to a large extent by how well they are able to accept the energy available from these high-current pulses. Better DCA performance means more charge accepted, which in turn equates to more efficient energy recovery. This is key to achieving longer battery life, and hence greater range, for EV's.

Increased understanding of DCA performance has been identified as an important contributor to the continuing development of automotive batteries [2]. A standard test procedure exists for characterising the DCA performance of batteries [3], and studies have been undertaken to determine how test parameters and environmental conditions affect DCA performance [4].

Whilst most efforts have focussed on DCA for automotive applications, the underlying principle has much wider applications and is important in any system where it is desirable for a battery to accept charge in a time-limited fashion. Such applications include grid-connected storage systems, particularly when operating in Enhanced Frequency Response (EFR) mode, and smaller scale renewable energy systems. Clearly then, a greater understanding of the factors influencing DCA performance, and methods for improving it could have broad applications across the whole energy storage sector.

It has previously been identified that reducing the rest period within the DCA test procedure improves charge acceptance [4]. This paper presents the results of an investigation to determine if a similar result could be achieved by injecting a sinusoidal ripple current at a higher frequency, but of a lesser magnitude than that used in the DCA test.

II. Battery Analysis

The batteries used in this study were RS Pro 698-8091 VRLA type, with a nominal voltage of 12 V and a rated capacity (C_{nom}) of 4 Ah. Before proceeding to the DCA testing phase, the batteries were analysed to determine their frequency response.

A. Spectroscopy

This analysis was performed using a Solartron Analytical 1260 + 1287 Electrochemical Impedance Spectroscopy (EIS) instrument, in conjunction with an environmentally controlled chamber to maintain the ambient temperature of the battery at 25°C throughout the analysis period.

Prior to performing the analysis the battery was discharged to 70 % State of Charge (SoC), this is the same as that at which the DCA testing was performed (see below for details) and the batteries rested. This ensures that the results of the spectroscopy are representative of the performance of the battery during the DCA test, as the frequency response will change with SoC [5]. The analysis was performed in a potentiostatic mode, after discharging to 70 % SoC the cell

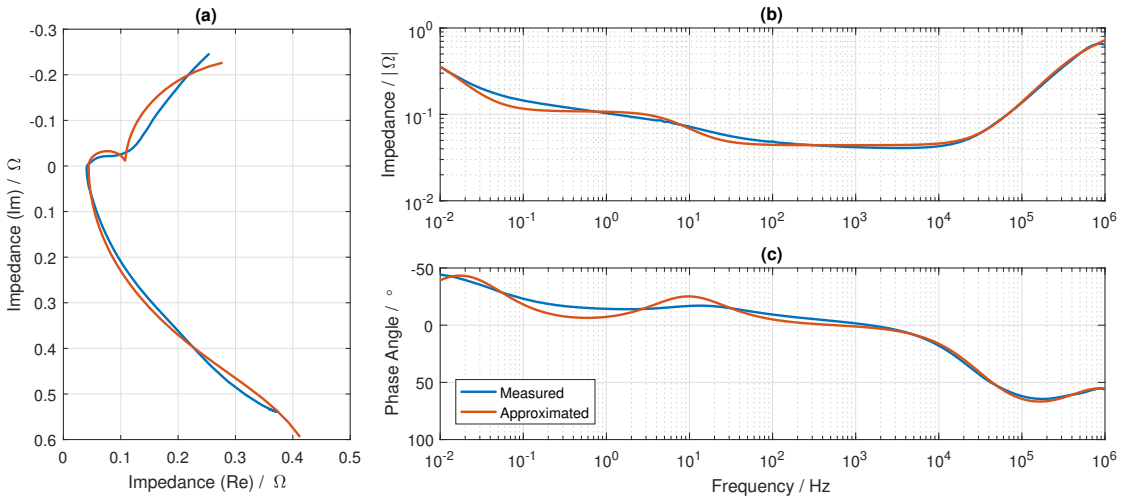

Fig. 1: EIS Spectra. (a) Nyquist Plot, (b) Bode Plot - Magnitude Response, (c) Bode Plot - Phase Response

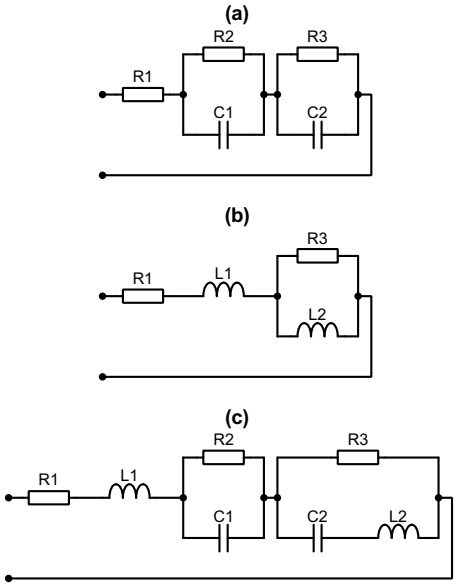

Fig. 2: Battery Equivalent Circuit Models. (a) Randles, (b) High frequency from [6], (c) Hybrid

TABLE I: Model Component Parameters

	Model		
Component	A	B	C
R_1	46.1 mΩ	41.1 mΩ	44.0 mΩ
R_2	63.7 mΩ	–	64.1 mΩ
R_3	530.0 mΩ	412.6 mΩ	472.0 mΩ
C_1	397.8 mF	–	398.2 mF
C_2	45.0 F	–	45.0 F
L_1	–	66.1 nH	63.5 nH
L_2	–	140.4 nH	141.8 nH

was rested for 10 hours to determine the open-circuit voltage (OCV), the test instrument then maintains this OCV potential throughout the test period.

Superimposed on the OCV potential is a sinusoidal ac voltage, this causes a current to flow in the battery which is measured by the test instrument. From the applied voltage and measured current the impedance of the battery is determined by the Solartron software. This process is performed repeatedly with the frequency of the applied voltage varying, in this way a spectrum is produced giving the impedance of the battery across a range of frequencies.

For this analysis the frequency range selected was 10 mHz – 1 MHz, using a logarithmic sweep with 20 points per decade. This being selected to be representative of both the low frequency components typical of the DCA test procedure as well as higher frequencies commonly produced by power-electronic switching devices. The range chosen also gives a wide spectrum which allows for a better understanding of the underlying performance of the battery. Figure 1 shows the results of the analysis, with the measured response shown in blue.

From the spectroscopy result it is clear that the behaviour of the battery can be separated into two regions. At low frequencies the response is capacitive, as indicated by $Im(Z)$ and the phase angle being negative. Conversely, at high frequencies $Im(Z)$ and the phase angle are positive, indicating an inductive response. The crossover frequency between these two regions occurs at around 1.5 kHz. To better understand the performance of the battery, each region was considered individually for modelling before the two models were combined to produce a full representation of the battery behaviour.

A commonly used electrical model for the low-frequency behaviour of a battery is the Randles model [7], this models the battery as a pair of series connected, parallel RC circuits, as shown in Figure 2a. Whilst improvements have been proposed [8], the basic Randles model is well regarded for its simplicity.

The software provided with the EIS instrument (*ZPlot & ZView 2*) allows for the fitting of models to measured data. When provided with an equivalent circuit and some initial parameter estimates, the software performs an iterative

fitting process to determine the component values which best approximate the measured data; i.e. the smallest weighted error between the measured and approximated frequency spectra. The results of this process for the Randles model applied to the measured frequency spectrum from 10 mHz – 1.5 kHz are given in Table I–A.

A high-frequency battery model is proposed by [6]. This replaces the capacitive elements of the Randles model with inductors and simplifies the parallel branches, to better represent the electrical appearance of the battery at higher frequencies. This model is shown in Figure 2b. The results of the fitting process using this high-frequency model applied to the measured frequency spectrum from 1.5 kHz – 1 MHz are given in Table I–B.

It may be seen that the components common to the models described above, R_1 & R_3, appear to have similar values. This is a good indication that the models are describing the same system but at different frequencies, as the resistive elements should perform the same regardless of frequency. Combining both models to produce a hybrid model results in the equivalent circuit given in Figure 2c. This is similar to previously described models [5], [9], [10], but with the reactive components replacing constant-phase elements.

Using the component values previously determined as a starting point and the whole measured frequency spectrum, the results of the fitting process for the hybrid model are given in Table I–C. The performance of this hybrid model to the same stimulus as the actual battery is shown by Figure 1, in orange. The similarities between the measured and approximated responses are clear and suggests the model is a reasonable description of the behaviour of the battery.

B. Ripple Frequency Selection

Aside from providing a model describing the behaviour of the battery, the spectroscopy results also allow for the selection of likely frequencies for affecting the performance of the battery. As the hybrid model includes both inductive and capacitive elements, this indicates that the battery will behave in a similar way to a resonant circuit.

As $f \to \infty$ the impedance of the inductors becomes the significant influence and the battery impedance will be dominated by that of L_1, this being in series with all other elements. As $f \to 0$, conversely, the capacitive elements dominate; as these are in parallel branches, the battery impedance will tend toward R_1 + R_2 + R_3.

This can clearly be seen from the impedance spectrum in Figure 1b, the impedance is relatively high at low frequency; as frequency increases, the impedance falls to a minimum at around 50 Hz. It then remains broadly flat until around 10 kHz, at which point the inductance becomes significant and the impedance rises rapidly.

The main charge storage elements of the battery are the capacitors, C_2 in particular, therefore in order to affect the performance of the battery as a whole it is important that the ripple current affects these elements. At low frequencies the bulk of the current will flow in the resistances, whilst at high frequencies although C_1 will be the favoured current path through the network of C_1 & R_2, L_2 will restrict current flow through C_2. Therefore, to maximise the current flow through the capacitive elements, the frequency should be be selected to lie in the range at which the total impedance of the battery is at a minimum.

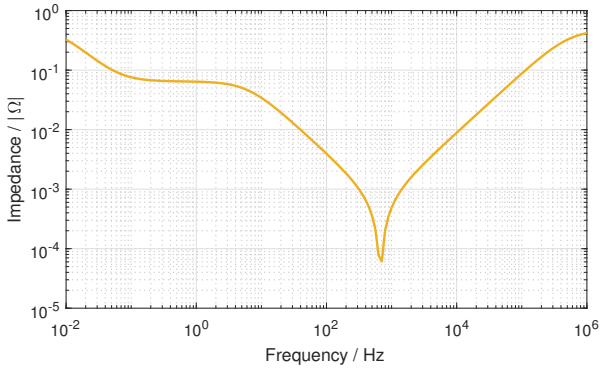

Fig. 3: Impedance Spectrum for Hybrid Model, Neglecting R_1 & L_1

The spectroscopy result given in Figure 1b shows the battery impedance to be at a minimum in the range of circa 50 Hz – 10 kHz. From this broad range it is unclear which frequency would be best for influencing the battery. R_1 & L_1 together model the impedance of the internal connections between the terminals and cells within the battery, as such they do not represent the performance of the charge storing structures. By neglecting these components a frequency spectrum for the charge storage elements alone may be produced, this is shown in Figure 3.

As can be seen, this much more closely resembles the classical resonant circuit impedance spectrum, with a clearly defined resonant frequency of around 700 Hz. This corresponds to the point of minimum impedance, and is therefore selected as the frequency of the ripple current used for the work presented below.

III. Test Procedure

The test procedure is based on previous work to determine how DCA performance is influenced by the test parameters, this work is reported in [4].

A. DCA Description

A full discussion of the DCA test procedure is beyond the scope of this paper, for full details see [3], [4]. Briefly, however, at the core of the DCA test is the microcycle. This is a specified current waveform which is applied to the battery, from its response to this stimulus the DCA performance may be determined. The microcycle used for this test, as modified from the DCA Test standard is shown in Figure 4 and summarised in Table II.

The key part of the microcycle is step 1, here the test applies a large charge pulse to the battery, causing its voltage to rise. If the voltage exceeds 14.8 V, the charge current is reduced

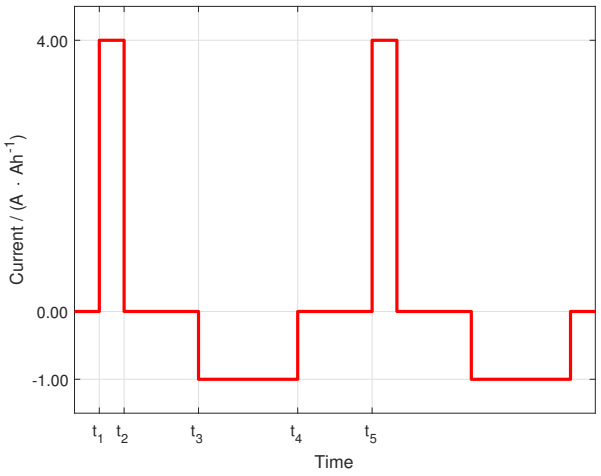

Fig. 4: DCA Test Microcycle Current Profile (t_1 – t_5)

TABLE II: DCA Test Microcycle Current Profile Procedure

Step	Description
1, (t_1 – t_2)	Charge at 4.00 A·Ah^{-1} with voltage limit of 14.8 V for 10 s
2, (t_2 – t_3)	Rest 300 s
3, (t_3 – t_4)	Discharge at 1.00 A·Ah^{-1}
4, (t_4 – t_5)	Rest 300 s

to maintain the voltage at the upper limit. This reduction in charge current will equate to a lower total amount of charge accepted for the microcycle. DCA is determined by the amount of charge the battery is able to accept as a fraction of the total amount theoretically available. The current levels used for the microcycle are normalised to the actual capacity of the battery C_{exp}, which is experimentally determined during the test procedure.

Each microcycle is charge-balanced, the amount of charge added to the battery in step 1 is removed during step 3, i.e:

$$\int_{t_1}^{t_2} I(t)\ dt = -\int_{t_3}^{t_4} I(t)\ dt \tag{1}$$

This is achieved by dynamically varying the length of the discharge step, and ensures that the SoC at the end of the microcycle is the same as it was at the start. The remaining sections of the microcycle run for fixed times as specified in Table II. The battery is subjected to 20 repetitions of the microcycle profile, this being one DCA Pulse Profile (DCAPP).

B. DCA Calculation

DCA is given in terms of the average recuperation current (I_{recu}) for the charge pulse [11], which has units of A·Ah^{-1}. Thus, for a pulse of arbitrary length, DCA is given by

$$I_{recu} = \frac{Ah_{recu} \cdot 3600}{C_{exp} \cdot t} \tag{2}$$

where Ah_{recu} is the amount charge accepted during the pulse in ampere-hours, C_{exp} is the capacity of the battery in ampere-hours and t is the length of the charge pulse in seconds.

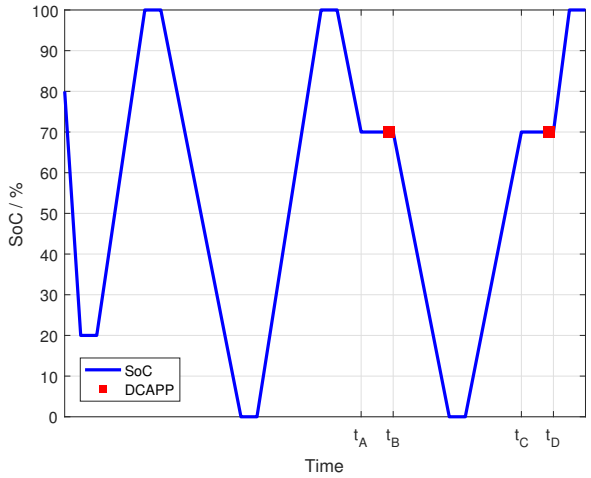

Fig. 5: Test Procedure SoC Profile & DCAPP Locations

C. Effect of History on DCA Performance

A critical factor influencing DCA performance, as identified by [4], is the operational history of the battery. This refers to the operations which have been performed on the battery prior to the DCA test and may be divided into discharge history (DH), where the battery has previously been discharged, and charge history (CH) where it was charged.

The effects of this history have been shown by [4] to be very significant, with large differences in DCA performance at the same SoC, dependant on the battery's history. It is crucial therefore that the this influence be accounted for in the test procedure.

D. Test Description

Figure 5 shows the SoC profile for the test procedure. This begins with a high-rate discharge to test the reserve capacity of the battery, followed by a 1-hour rest and recharge to 100 % SoC. The battery is then discharged to 0 % SoC at the 5-hour rate, from this C_{exp} is determined. From this point the battery is then fully recharged, rested and discharged to 70 % SoC. Following another 1-hour rest the first DCAPP is performed, this testing the DCA performance when the battery has discharge history. For the duration of the DCAPP and the rest period leading up to it (t_A – t_B), a sinusoidal ripple current of 1.6 A_{RMS}, equivalent to 0.4C_{nom}, at 700 Hz is applied to the battery.

The battery is then fully discharged, rested and recharged to 70 % SoC. Again, after resting for 1-hour a second DCAPP is performed, testing the DCA performance with charge history. As before the ripple current is applied for the duration of the DCAPP procedure and the rest preceding it, t_C – t_D.

IV. Results & Discussion

To establish a baseline performance, the test procedure described above was applied to the battery under test, but without any injected ripple. The battery performance under these conditions is shown in Figure 6, in blue. This figure shows the average charge acceptance for each of the 20

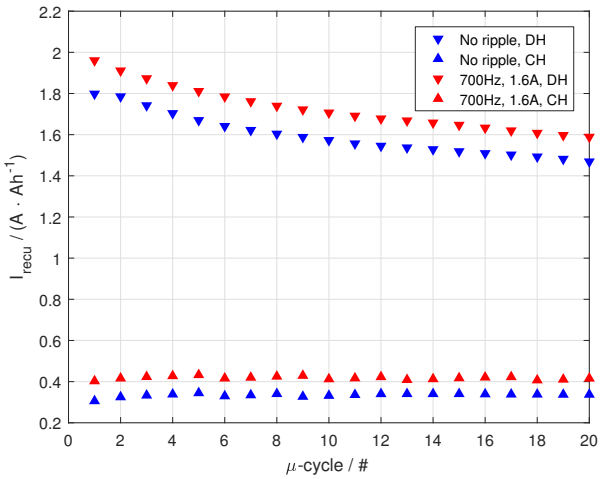

Fig. 6: DCA Analysis Result - Effect of Injected Ripple Current

microcycles of the DCAPP, with charge and discharge history, this shows the typical DCA performance traits as identified by [4].

The first and most obvious of these is the large difference in performance dependant on the operational history of the battery; with discharge history the performance is significantly better than when the battery has charge history. Secondly, the history influences the performance as the DCAPP progresses in different ways, with discharge history there is a general decrease in charge acceptance as the number of microcycles increases, whilst with charge history the performance is broadly consistent across the whole DCAPP.

Figure 6 also shows the DCA performance of the battery when subjected to the full test procedure with the 1.6 A_{RMS} ripple current applied. It may be clearly seen from this figure that the injection of a ripple current improves the charge acceptance performance of the battery. The result shows the same traits as identified for the baseline are present, but in all

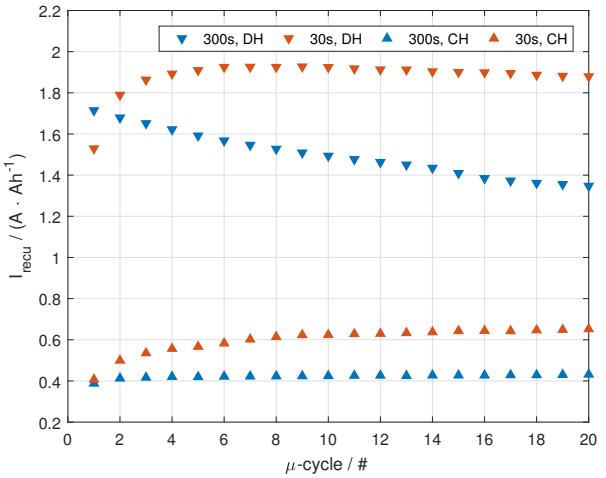

Fig. 7: DCA Analysis Result - Effect of Reduced Rest Period

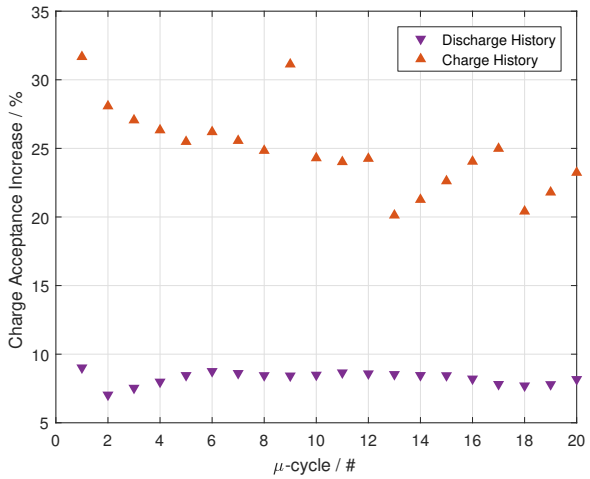

Fig. 8: Charge Acceptance Improvement with Applied Ripple Current

TABLE III: Average Charge Acceptance Improvement with Applied Ripple Current

History	Increase
Discharge	8.26 %
Charge	24.87 %

cases the amount of charge accepted is greater.

This differs from the effect previously observed when the rest period was reduced, in those cases whilst DCA performance was improved, the trend of changing charge acceptance within the DCAPP was also altered; tending to increase as the number of microcyles increased [4]. This is illustrated by Figure 7, which shows the effect on the DCA performance of a VRLA cell when the rest period is reduced from 300s as used in this test, to 30s; the data being taken from [4].

Comparing the results given in Figure 7 with those observed from this study (Figure 6), it may be seen that the effect produced by the injected ripple current is very different to that caused by reducing the rest period. Whilst both methods improve DCA performance, the injected ripple current does not alter the trend of charge acceptance within the DCAPP as reducing the rest period does.

The nature of the improvement seen is illustrated by Figure 8, which shows the percentage increase in charge acceptance over the baseline for each microcycle. This result is of particular interest as it shows a significantly larger improvement in performance when the battery has charge history, this is important as the overall charge acceptance is much poorer in this case, so this larger improvement will be more beneficial to the performance of the battery.

For completeness, Table III gives the average performance improvement for the compete DCAPP observed in this study.

V. Conclusions & Further Work

The work has shown that the application of ripple currents to lead-acid batteries can improve their DCA performance by

around 25 %. This is interesting and exciting, however there is much more work to be done.

Thus far the work has only shown results for a single battery and at a single frequency, clearly it is necessary to expand the investigation to cover more batteries of the same type at a variety of frequencies as well as different chemistries to get a fuller understanding of the effects of ripple currents.

Another area which must be investigated is the effect of the ripple current on the SoC of the battery. As the round-trip efficiency of the battery is less than 100 %, not all of the energy removed during the negative half-cycle will be returned during the positive half, even if the currents in both are equal. Whilst the net loss of charge per cycle will be negligible, over time the cumulative effect will be a reduction of SoC, which will become more significant the longer the ripple is applied. It will be necessary to quantify this loss and thus adjust the ripple current waveform such that is energy-balanced, if this problem is to be avoided.

Despite these shortcomings however, the work presented above appears to show that it is possible to improve DCA performance by applying ripple currents, and furthermore that magnitude of the currents required are relatively modest when compared to those typically found in EV & HEV applications.

REFERENCES

[1] P. T. Moseley and D. A. Rand, "Partial state-of-charge duty: A challenge but not a show-stopper for lead-acid batteries!" *ECS Transactions*, vol. 41, no. 13, pp. 3–16, 2012.

[2] E. Karden, S. Ploumen, B. Fricke, T. Miller, and K. Snyder, "Energy storage devices for future hybrid electric vehicles," *Journal of Power Sources*, vol. 168, no. 1, pp. 2–11, 2007.

[3] European Committee for Electrotechnical Standardisation, "EN 50342-6:2015. Lead-acid starter batteries - Part 6: Batteries for Micro-Cycle Applications," November 2015.

[4] M. Smith, D. Gladwin, and D. Stone, "Experimental analysis of dynamic charge acceptance test conditions for lead-acid and lithium iron phosphate cells," *Journal of Energy Storage*, vol. 12, pp. 55–65, 2017.

[5] S. Buller, M. Thele, R. W. De Doncker, and E. Karden, "Impedance-based simulation models of supercapacitors and li-ion batteries for power electronic applications," in *Industry Applications Conference, 2003. 38th IAS Annual Meeting. Conference Record of the*, vol. 3. IEEE, 2003, pp. 1596–1600.

[6] J. Wang, K. Zou, C. Chen, and L. Chen, "A high frequency battery model for current ripple analysis," in *Applied Power Electronics Conference and Exposition (APEC), 2010 Twenty-Fifth Annual IEEE*. IEEE, 2010, pp. 676–680.

[7] K. Vetter, *Elektrochemische Kinetik. (German) [Electrochemical Kinetics]*. Springer, Berlin, 1961.

[8] C. R. Gould, C. M. Bingham, D. A. Stone, and P. Bentley, "New battery model and state-of-health determination through subspace parameter estimation and state-observer techniques," *Vehicular Technology, IEEE Transactions on*, vol. 58, no. 8, pp. 3905–3916, 2009.

[9] D. A. Howey, P. D. Mitcheson, V. Yufit, G. J. Offer, and N. P. Brandon, "Online measurement of battery impedance using motor controller excitation," *IEEE transactions on vehicular technology*, vol. 63, no. 6, pp. 2557–2566, 2014.

[10] D. Howey, V. Yufit, P. Mitcheson, G. Offer, and N. Brandon, "Impedance measurement for advanced battery management systems," in *Electric Vehicle Symposium and Exhibition (EVS27), 2013 World*. IEEE, 2013, pp. 1–7.

[11] H. Budde-Meiwes, D. Schulte, J. Kowal, D. U. Sauer, R. Hecke, and E. Karden, "Dynamic charge acceptance of lead–acid batteries: Comparison of methods for conditioning and testing," *Journal of Power Sources*, vol. 207, pp. 30–36, 2012.